Analysis of Capacitive Impedance Matching Networks for Simultaneous Wireless Power Transfer to Multiple Devices

Jinwook Kim, *Member, IEEE*, Do-Hyeon Kim, *Student Member, IEEE*, and Young-Jin Park, *Member, IEEE*

***Abstract*—This paper presents wireless power transfer (WPT) characteristics according to load variation in multi-device WPT systems using capacitive impedance matching networks (IMNs). Two basis IMNs of using series–parallel (SP) capacitors and parallel–series (PS) capacitors are used. Four combinations of capacitive IMNs are considered, i.e., SP in a transmitting side and SP in a receiving (Rx) side (SP-SP), SP-PS, PS-SP, and PS-PS. The optimum capacitance values for each IMN are also derived by circuit analysis. For verification, three cases based on the number of Rx coils are considered, and the calculated results are compared with the simulated and measured results for each case. A WPT system for only a single device has identical power transfer efficiency for four combinations of the IMNs. Multidevice WPT systems with the PS IMN in Rx sides are found to transfer more power toward the Rx coil with lower load impedance according to the load variation. On the other hand, using the SP IMN in Rx sides is less sensitive to load variation than using the PS IMN. In addition, a WPT system using the PS-PS IMN combination is less responsive to the cross coupling between Rx coils than that using the SP-SP IMN combination.**

***Index Terms*—Capacitive impedance matching, cross coupling, loosely coupled coils, multiple devices, wireless power transfer (WPT).**

I. Introduction

IMPEDANCE matching networks (IMNs) are essential for increasing power transfer efficiency in wireless power transfer (WPT) using magnetic fields [1], [2]. IMNs using only capacitors are widely used. In particular, IMNs using series or parallel resonant capacitors in transmitting (Tx) and receiving (Rx) coils, which are called as S-S, S-P, P-S, or P-P IMNs, have been often adopted in WPT systems [3]–[10]. It is possible to increase the power transfer efficiency by eliminating reactance in the WPT system. In addition, the S-S IMN allows us to be able to analyze the WPT system intuitively. However, by using the S-S IMN only, it is difficult to perfectly match the impedance at both Tx and Rx sides simultaneously.

IMNs, including inductors and capacitors, in series and parallel have been also reported [11]–[13]. However, at a higher frequency, the inductors in the IMNs are likely to be too bulky to be built in portable devices and make ohmic loss increase [11]. Hence, capacitive IMNs of combining series and parallel capacitors without inductors, i.e., series–parallel (SP) compensation or parallel–series (PS) compensation IMNs, are widely used in WPT systems. SP and PS IMNs have been also adopted in two representative global standardizations of Alliance for Wireless Power Consortium (A4WP) [14] and Wireless Power Consortium (WPC) [15]. Different operating frequencies in the standardizations are used, but they recommend SP and PS networks as IMNs. In addition, many research studies have been reported using SP and PS IMNs [16]–[19]. However, there is little information on the characteristics of IMNs with the combination of SP and PS networks, i.e., SP-SP, SP-PS, PS-SP, and PS-PS.

One important feature of magnetic resonance WPT is that multiple devices can be simultaneously recharged by using one Tx coil [6]–[9], [15], [20]–[24]. Hence, the WPT has been studied in many applications such as smart phones [12] and laptops [2]. In general, lithium-ion (Li-Ion) rechargeable batteries in portable electronic devices are charged at constant current (CC) until the battery voltage reaches the peak cell voltage and then are charged at constant voltage (CV) [25]. Due to this charging process, the battery can be regarded as a variable load depending on the charging capacity [4], [14]. Since undesired load variation causes efficiency degradation of WPT systems [14], the influence due to the load variation should be considered when multiple devices with different battery charging capacities are charged simultaneously.

In this paper, WPT systems with capacitive IMNs of SP and PS networks for charging multiple devices are analyzed in terms of power transfer efficiency and power division. Optimum capacitance values for perfect impedance matching are also derived. The power transfer efficiency and power division ratio among multiple devices considering the load variation are shown and compared according to the IMNs.

II. Analysis of a WPT System for Charging Multiple Devices Using Capacitive IMNs

A. WPT System for Charging Multiple Devices

Fig. 1 shows an equivalent circuit of a WPT system for charging multiple devices with IMNs at both the Tx and Rx. R_t and L_t denote the resistance and self-inductance, respectively,

Manuscript received April 7, 2014; accepted October 1, 2014. Date of publication October 29, 2014; date of current version April 8, 2015. This work was supported by the Primary Research Program of the Korea Electrotechnology Research Institute funded by the Ministry of Science, ICT and Future Planning under Grant 14-12-N0101-08.

J. Kim was with the University of Science and Technology, Ansan 426-910, Korea. He is currently with the Korea Electrotechnology Research Institute, Ansan 426-910, Korea (e-mail: jwkim@ust.ac.kr).

D.-H. Kim and Y.-J. Park are with the University of Science and Technology, Ansan 426-910, Korea, and also with the Korea Electrotechnology Research Institute, Ansan 426-910, Korea (e-mail: yjpark@keri.re.kr).

Color versions of one or more of the figures in this paper are available online at http://ieeexplore.ieee.org.

Digital Object Identifier 10.1109/TIE.2014.2365751

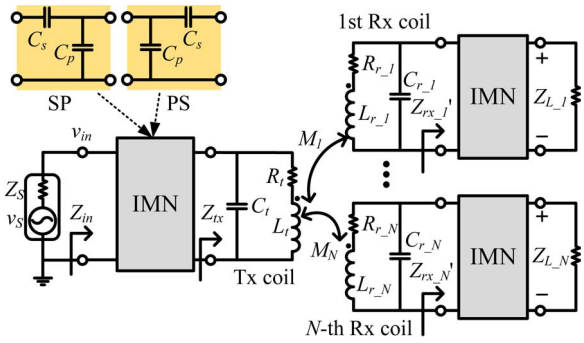

Fig. 1. Configuration of a WPT system for multiple devices using combinations of two capacitive IMNs of SP compensation and PS compensation.

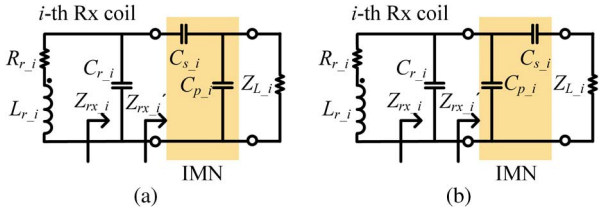

Fig. 2. Equivalent circuit of the ith Rx coil in Fig. 1 (a) with the SP IMN and (b) with the PS IMN at Rx.

of the Tx coil, whereas R_r and L_r represent those of an Rx coil. N is the number of devices. Each Rx coil is inductively coupled to the Tx coil with mutual inductance, i.e., $M_i (i = 1, \ldots, N)$. For theoretical derivation, cross couplings between Rx coils are neglected. In Section III-E, simulation and measurement considering the cross couplings will be shown. Z_S is the characteristic impedance of a source. $Z_{L\_i} (i = 1, \ldots, N)$ denotes an equivalent load impedance of the ith Rx coil looking into a load from the IMN. The load may include a rectifier, a dc/dc converter, a battery charger, and a Li-Ion battery. In this paper, the equivalent load impedance is assumed to be variable real impedance in the same manner of previous studies [4], [14], [17]. For impedance matching at both Tx and Rx sides, SP or PS IMNs are adopted.

B. Circuit Analysis of an Rx Coil With SP or PS IMNs

Fig. 2(a) and (b) shows an equivalent circuit of the ith Rx coil with SP and PS IMNs, respectively, in Fig. 1. The Rx impedance looking into the load impedance Z'_{rx_i} at the ith Rx coil with SP and PS IMNs are, respectively, as follows:

$$Z'_{rx\_i}|_{SP} = \frac{Z_{L\_i}}{1+\omega^2 C_{p\_i}^2 Z_{L\_i}^2} - j\left(\frac{\omega C_{p\_i} Z_{L\_i}^2}{1+\omega^2 C_{p\_i}^2 Z_{L\_i}^2} + \frac{1}{\omega C_{s\_i}}\right) \quad (1)$$

$$Z'_{rx\_i}|_{PS} = \frac{Z_{L\_i} - j\left[\omega C_{p\_i} Z_{L\_i}^2 + \frac{1}{\omega C_{s\_i}}\left(1+\frac{C_{p\_i}}{C_{s\_i}}\right)\right]}{\left(1+\frac{C_{p\_i}}{C_{s\_i}}\right)^2 + \omega^2 C_{p\_i}^2 Z_{L\_i}^2}. \quad (2)$$

The loading impedance, including the parasitic capacitance C_{r_i} of the ith Rx coil, is given by

$$Z_{rx\_i} \equiv A_i + jB_i = \frac{\mathrm{Re}\left(Z'_{rx\_i}\right) + j\left[\mathrm{Im}\left(Z'_{rx\_i}\right) - \omega C_{r,i}\left|Z'_{rx\_i}\right|^2\right]}{1-2\omega C_{r\_i}\mathrm{Im}\left(Z'_{rx\_i}\right)+\omega^2 C_{r\_i}^2\left|Z'_{rx\_i}\right|^2}. \quad (3)$$

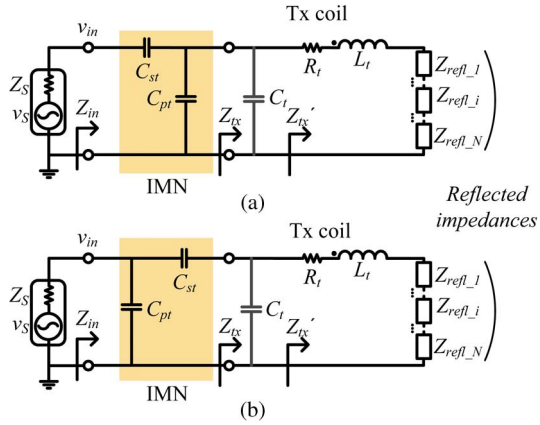

Fig. 3. Equivalent circuit of a Tx coil in Fig. 1 with the reflected impedance of Rx coils. (a) With the SP IMN and (b) with the PS IMN at Tx.

Here, $\mathrm{Re}(x)$ and $\mathrm{Im}(x)$ denote the real and imaginary of x, respectively.

C. Circuit Analysis of a Tx Coil With SP or PS IMNs

Input impedance at a Tx coil, including the reflected impedance of Rx coils, as shown in Fig. 3, Z'_{tx} is as follows:

$$Z'_{tx} = R_t + j\omega L_t + \sum_{i=1}^{N} Z_{\mathrm{refl\_}i} \quad (4)$$

where the reflected impedance of the ith Rx coil $Z_{\mathrm{refl\_}i}$ is given by

$$Z_{\mathrm{refl\_}i} = \frac{\omega^2 M_i^2}{R_{r\_i} + j\omega L_{r\_i} + Z_{rx\_i}}. \quad (5)$$

Therefore, the input impedance at the Tx coil, including parasitic capacitance C_t, Z_{tx} is written from (4) as follows:

$$Z_{tx} = \frac{\mathrm{Re}\left(Z'_{tx}\right) + j\left[\mathrm{Im}\left(Z'_{tx}\right) - \omega C_t\left|Z'_{tx}\right|^2\right]}{1-2\omega C_t \mathrm{Im}\left(Z'_{tx}\right)+\omega^2 C_t^2\left|Z'_{tx}\right|^2}. \quad (6)$$

From (6), the input impedance at a source is, according to SP and PS IMNs, given by

$$Z_{\mathrm{in}} = \begin{cases} \frac{1+j\omega(C_{st}+C_{pt})Z_{tx}}{j\omega C_{st}-\omega^2 C_{st}C_{pt}Z_{tx}}, & \text{for SP network} \\ \frac{1+j\omega C_{st}Z_{tx}}{j\omega(C_{st}+C_{pt})-\omega^2 C_{st}C_{pt}Z_{tx}}, & \text{for PS network} \end{cases} \quad (7)$$

where C_{st} and C_{pt} denote series and parallel capacitance values, respectively. Then, the transmission coefficient at a source is

$$T = \frac{2Z_{\mathrm{in}}}{Z_{\mathrm{in}} + Z_S}. \quad (8)$$

Here, the characteristic impedance of the source Z_S is assumed to be real impedance. From (8), the input voltage is as follows:

$$V_{\mathrm{in}} = TV_S. \quad (9)$$

From (7)–(9), the input power at a source is derived as follows:

$$P_{\mathrm{in}} = \mathrm{Re}\left(\frac{V_{\mathrm{in}} I_{\mathrm{in}}^*}{2}\right) = \frac{|T|^2|V_S|^2}{2}\mathrm{Re}\left(\frac{1}{Z_{\mathrm{in}}^*}\right). \quad (10)$$

Since power transfer efficiency can be obtained by the ratio of real impedances, the power transfer efficiency from the source

to the load of the ith Rx coil can be achieved as follows:

$$\begin{aligned}\eta_{rx\_i} &= \eta_S \eta_t \eta_{r\_i} \\ &= |T|^2 Z_S \mathrm{Re}\left(\frac{1}{Z_S^*}\right) \times \frac{\mathrm{Re}(Z_{\mathrm{refl}\_i})}{R_t + \sum_{i=1}^{N} \mathrm{Re}(Z_{\mathrm{refl}\_i})} \\ &\quad \times \frac{\mathrm{Re}(Z_{rx\_i})}{R_{r\_i} + \mathrm{Re}(Z_{rx\_i})} \end{aligned} \tag{11}$$

where $\eta_S = P_{\mathrm{in}}/P_S$, with $P_S = V_S^2/(2Z_S)$. η_t and η_{r_i} represent the ratios between the resistance and reflected impedances at the Tx coil in Fig. 3 and between the resistance and real impedance at the ith Rx coil, respectively. Received power at the ith load can be obtained as follows:

$$P_{L\_i} = \eta_{rx\_i} P_S. \tag{12}$$

The total power transfer efficiency is achieved by adding all power transfer efficiency values of (11) as follows:

$$\eta = \sum_{i=1}^{N} \eta_{rx\_i}. \tag{13}$$

D. Optimum Conditions in a Multidevice WPT System

To maximize power transfer efficiency for N Rx coils, the following conditions of A_i and B_i should be satisfied [20]:

$$A_i^{\mathrm{opt}} = R_{r\_i} \sqrt{1 + \sum_{i=1}^{N} \left(\frac{\omega^2 M_i^2}{R_t R_{r\_i}}\right)} \tag{14}$$

$$B_i^{\mathrm{opt}} = -\omega L_{r,i}. \tag{15}$$

When $Z_{rx\_i} = A_i^{\mathrm{opt}} + jB_i^{\mathrm{opt}}$, Z_{tx} with optimum Z_{rx_i} is rewritten from (4)–(6) as follows:

$$\mathrm{Re}\left(Z_{tx}^{\mathrm{opt}}\right) = \frac{R_t + \sum_{i=1}^{N} Z_{\mathrm{refl}\_i}^{\mathrm{opt}}}{\left(1-\omega^2 C_t L_t\right)^2 + \omega^2 C_t^2 \left(R_t + \sum_{i=1}^{N} Z_{\mathrm{refl}\_i}^{\mathrm{opt}}\right)^2} \tag{16}$$

$$\mathrm{Im}\left(Z_{tx}^{\mathrm{opt}}\right) = \frac{\omega L_t - \omega C_t \left[\omega^2 L_t^2 + \left(R_t + \sum_{i=1}^{N} Z_{\mathrm{refl}\_i}^{\mathrm{opt}}\right)^2\right]}{\left(1-\omega^2 C_t L_t\right)^2 + \omega^2 C_t^2 \left(R_t + \sum_{i=1}^{N} Z_{\mathrm{refl}\_i}^{\mathrm{opt}}\right)^2} \tag{17}$$

where

$$Z_{\mathrm{refl}\_i}^{\mathrm{opt}} = \frac{\omega^2 M_i^2}{R_{r\_i} + A_i^{\mathrm{opt}}}. \tag{18}$$

E. Optimum Capacitance Values for SP or PS IMNs

For the optimum conditions, $A_i = A_i^{\mathrm{opt}}$ and $B_i = B_i^{\mathrm{opt}}$, the optimum capacitance values for the ith Rx coil with an SP IMN are derived by simple circuit analysis using (1)–(3) as follows:

$$C_{p\_i}\Big|_{SP} = \pm \frac{1}{\omega Z_{L\_i}} \sqrt{\frac{Z_{L\_i}}{A_i^{\mathrm{opt}}} - 1} \tag{19}$$

$$C_{s\_i}\Big|_{SP} = \frac{1}{\omega \left[\omega L_{r\_i} \mp A_i^{\mathrm{opt}} \sqrt{\left(\frac{Z_{L\_i}}{A_i^{\mathrm{opt}}} - 1\right)}\right]}. \tag{20}$$

By substituting (16)–(18) into (7) and using the conditions of $\mathrm{Re}(Z_{\mathrm{in}}^*) = Z_S$ and $\mathrm{Im}(Z_{\mathrm{in}}^*) = 0$, the optimum capacitance values for Tx are also obtained as follows:

$$C_{pt}\Big|_{SP} = \frac{\mathrm{Im}\left(Z_{tx}^{\mathrm{opt}}\right) \pm \sqrt{\frac{\mathrm{Re}\left(Z_{tx}^{\mathrm{opt}}\right)}{Z_S} \left|Z_{tx}^{\mathrm{opt}}\right|^2 - \left(\mathrm{Re}\left(Z_{tx}^{\mathrm{opt}}\right)\right)^2}}{\omega \left|Z_{tx}^{\mathrm{opt}}\right|^2} \tag{21}$$

$$C_{st}\Big|_{SP} = \frac{\mp \mathrm{Re}\left(Z_{tx}^{\mathrm{opt}}\right)}{\omega Z_S \sqrt{\frac{\mathrm{Re}\left(Z_{tx}^{\mathrm{opt}}\right)}{Z_S} \left|Z_{tx}^{\mathrm{opt}}\right|^2 - \left(\mathrm{Re}\left(Z_{tx}^{\mathrm{opt}}\right)\right)^2}} \tag{22}$$

where

$$\left|Z_{tx}^{\mathrm{opt}}\right|^2 = \left(\mathrm{Re}\left(Z_{tx}^{\mathrm{opt}}\right)\right)^2 + \left(\mathrm{Im}\left(Z_{tx}^{\mathrm{opt}}\right)\right)^2. \tag{23}$$

In a similar way, for the PS IMN, the optimum capacitance values for the ith Rx coil and the Tx coil are written, respectively, as follows:

$$C_{p\_i}\Big|_{PS} = \frac{\omega L_{r\_i} \pm \sqrt{\frac{A_i^{\mathrm{opt}}}{Z_{L\_i}} \left[\left(A_i^{\mathrm{opt}}\right)^2 + \left(B_i^{\mathrm{opt}}\right)^2\right] - \left(A_i^{\mathrm{opt}}\right)^2}}{\omega \left[\left(A_i^{\mathrm{opt}}\right)^2 + \left(B_i^{\mathrm{opt}}\right)^2\right]} \tag{24}$$

$$C_{s\_i}\Big|_{PS} = \frac{A_i^{\mathrm{opt}}}{\mp \omega Z_{L\_i} \sqrt{\frac{A_i^{\mathrm{opt}}}{Z_{L\_i}} \left[\left(A_i^{\mathrm{opt}}\right)^2 + \left(B_i^{\mathrm{opt}}\right)^2\right] - \left(A_i^{\mathrm{opt}}\right)^2}} \tag{25}$$

$$C_{st}\Big|_{PS} = \frac{1}{\omega}\left[\mathrm{Im}\left(Z_{tx}^{\mathrm{opt}}\right) \mp \mathrm{Re}\left(Z_{tx}^{\mathrm{opt}}\right) \sqrt{\left(\frac{Z_S}{\mathrm{Re}\left(Z_{tx}^{\mathrm{opt}}\right)} - 1\right)}\right]^{-1} \tag{26}$$

$$C_{pt}\Big|_{PS} = \pm \frac{1}{\omega Z_S} \sqrt{\frac{Z_S}{\mathrm{Re}\left(Z_{tx}^{\mathrm{opt}}\right)} - 1}. \tag{27}$$

In both IMNs, sign of C_p and C_s should be chosen properly to be positive values simultaneously. The minus sign means that inductance is necessary to match the impedance. Hence, when the sign of C_p and C_s is minus, the inductance of $(-1/\omega^2 C)$ should be replaced with the capacitance for perfect impedance matching. That is, there is a limitation of the IMN using only SP and PS.

III. Experimental Results

A. Measurement of Power Transfer Efficiency Values of Multiple Devices for Load Variation Using a Two-Port VNA

Power transfer efficiency values from a source to a load of each device are measured using an Agilent 4395A two-port vector network analyzer (VNA) [26]. In Fig. 4, a schematic for measurement is presented. The unmeasured ports are connected with termination loads in measuring the power transfer efficiency from a source to a load.

When the load impedance of an Rx coil in measurement is not 50 Ω, i.e., 24 Ω or 150 Ω, the power transfer efficiency can be extracted using Agilent Advanced Design System (ADS) 2008 by using scattering parameters (S-parameters) measured

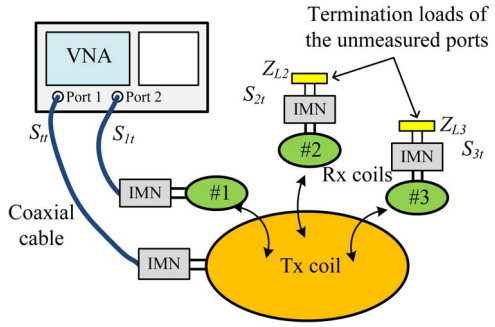

Fig. 4. Schematic of the efficiency measurement using a two-port VNA for a multidevice WPT system.

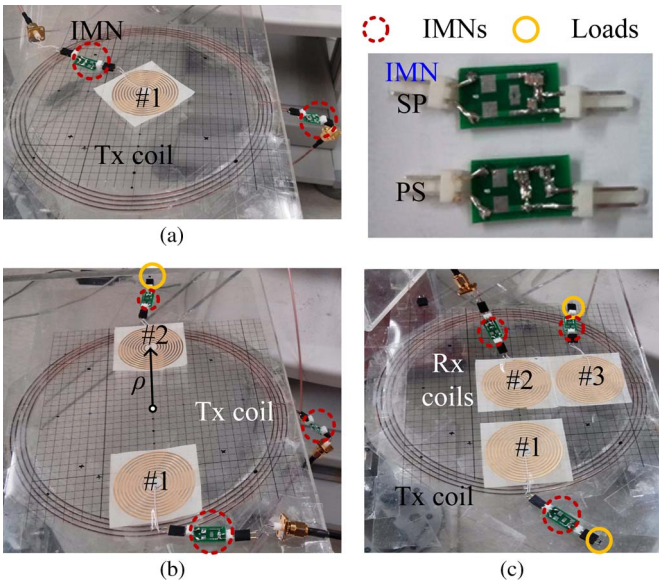

Fig. 5. Measurement setup with Tx and Rx coils. (a) Case 1: $N = 1$ with $\rho_1 = 0$. (b) Case 2: $N = 2$ with $\rho_1 = \rho_2 = 60$ mm. (c) Case 3: $N = 3$ with $\rho_1 = 60$ mm, $\rho_2 = 0$, and $\rho_3 = 50$ mm.

when the load impedance is 50 Ω. In multidevice WPT systems, since the characteristics from a Tx to an Rx are the main concern, overall N measurements are necessary for N Rx coils.

At first, S-parameters between the Tx coil and Rx coil #1, including IMNs, can be achieved when the others are terminated by proper load impedances. In a similar way, measurements of S-parameters between the Tx coil and Rx coil #2 and the Tx coil and Rx coil #3 are also performed when the unmeasured Rx coils are terminated with their load impedances. In Fig. 4, S_{tt} denotes the reflection coefficient at Tx. S_{1t}, S_{2t}, and S_{3t} denote S-parameters from the Tx to Rx coils #1, #2, and #3, respectively. The power transfer efficiency of the ith Rx coil is obtained by $|S_{it}|^2$ using the measured S-parameters. In the measurement, 1608-size RF chip resistors are used for the termination loads.

B. Fabrication of Tx and Rx Coils

Fig. 5 shows the measurement setup with the fabricated Tx and Rx coils. The Tx coil is a circular concentric multiloop coil with 4 turns, 3-mm pitch, and 90-mm radius. The Tx coil is made of a copper wire of 0.64-mm diameter. The Rx coil

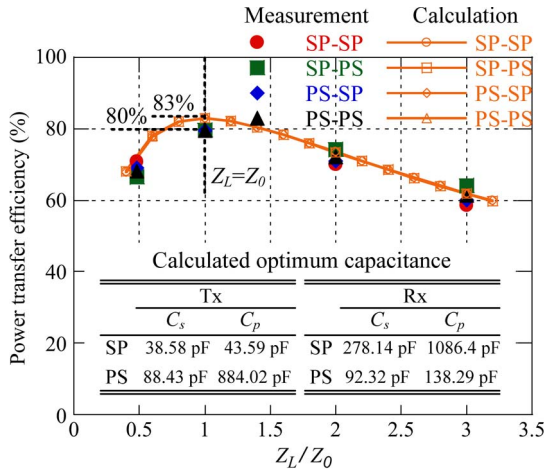

Fig. 6. Comparison of calculated and measured power transfer efficiency values with four IMNs according to variation of the normalized load impedance in case 1.

is a planar circular spiral coil with 10 turns, 2-mm pitch, and 23.5-mm radius. All Rx coils are identical and made of printed circuit board with a rectangular cross section of 1 mm × 0.2 mm.

Three different cases are considered in the experiment. Fig. 5(a) shows the measurement setup for WPT to a single device where only Rx coil #1 is placed at the center. Fig. 5(b) is the setup for WPT to two devices with the same radial displacement where both Rx coils #1 and #2 are placed at $\rho = 60$ mm. Fig. 5(c) shows WPT to three devices with different positions where Rx coils #1, #2, and #3 are placed at $\rho = 60$ mm, 0, and 50 mm, respectively.

The operating frequency of 6.78 MHz is used. A VNA, Agilent 4395A, is used to measure resistances of coils. An LCR meter, GW Instek G8110G, is used to measure self- and mutual inductances of coils. The measured resistance, self-inductance, and parasitic capacitance of the Tx coil are 0.919 Ω, 6.332 μH, and 5 pF, respectively, whereas those of an Rx coil are 0.704 Ω, 2.361 μH, and 4.5 pF, respectively. The gap between the Tx and Rx coils in all cases is 12 mm. Measured mutual inductances between the Tx and Rx coils are 201 nH at $\rho = 0$, 269 nH at $\rho = 50$ mm, and 305 nH at $\rho = 60$ mm.

C. Case 1 (WPT to a Device)

Fig. 6 shows calculated and measured power transfer efficiency values with four IMNs with combinations of SP-SP, SP-PS, PS-SP, and PS-PS according to variations in normalized load impedance Z_L/Z_0. An initial load impedance for impedance matching Z_0 is 50 Ω. Optimum capacitance values calculated by considering parasitic capacitance values of Tx and Rx coils are also shown in Fig. 6. The optimum capacitance values are obtained when $Z_L = Z_0$. Hence, the results show that power transfer efficiency values are maximal at $Z_L = Z_0$ and decrease with the load variation. The difference in the calculated and measured power transfer efficiency values is 3% when $Z_L = Z_0$. In addition, the calculated efficiency values with four IMNs are the same irrespective of the load variation. This means that the power transfer efficiency is not affected depending on the IMNs in WPT to a single device.

Calculated optimum capacitance

	Tx		Rx	
	C_s	C_p	C_s	C_p
SP	56.50 pF	25.81 pF	297.78 pF	659.15 pF
PS	89.90 pF	498.06 pF	136.60 pF	97.15 pF

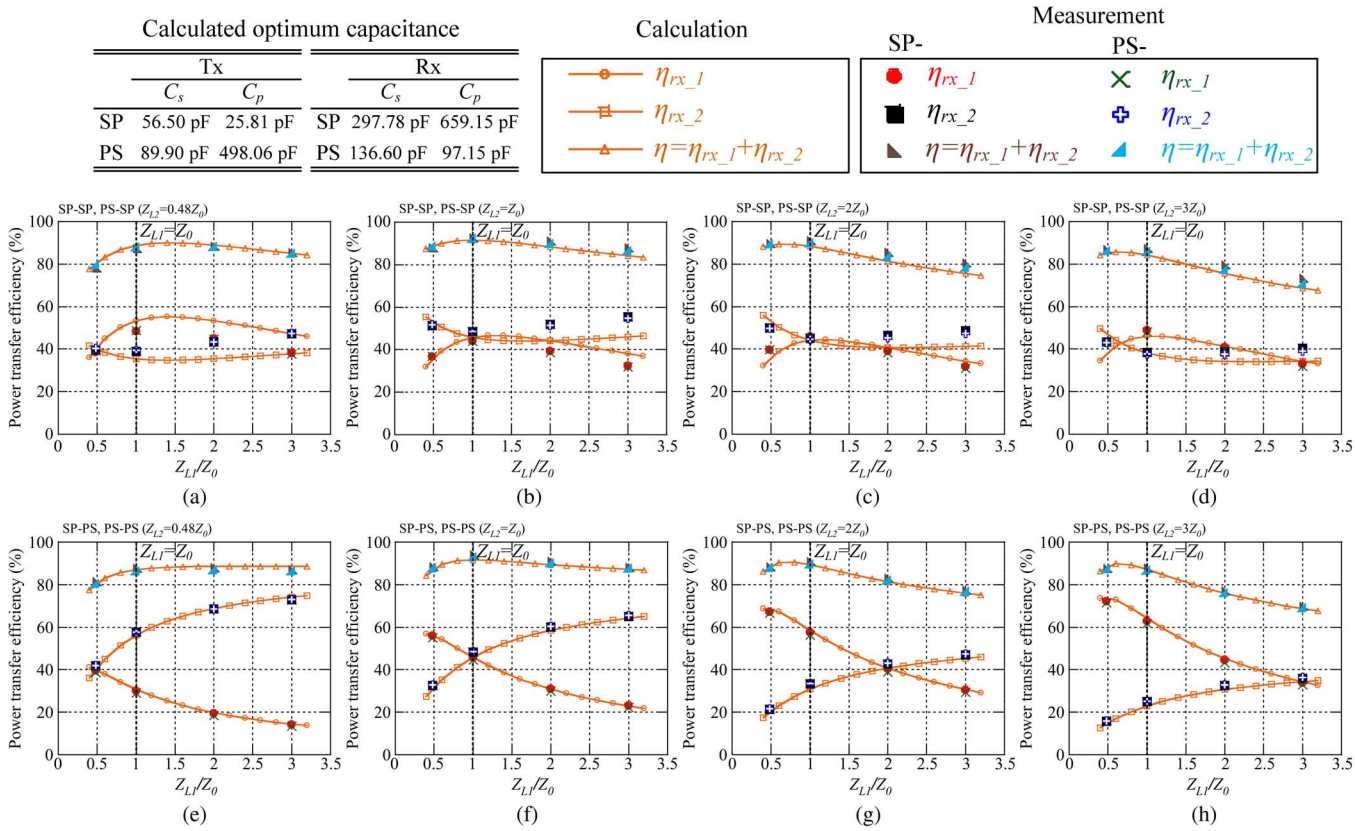

Fig. 7. Calculation and measurement of power transfer efficiency for case 2 according to the normalized load variation of Rx coil #1, Z_{L1}/Z_0, with the SP IMN at Rx sides where (a) $Z_{L2} = 0.48Z_0$, (b) $Z_{L2} = Z_0$, (c) $Z_{L2} = 2_{Z0}$, and (d) $Z_{L2} = 3Z_0$, and with the PS IMN at Rx sides where (e) $Z_{L2} = 0.48Z_0$, (f) $Z_{L2} = Z_0$, (g) $Z_{L2} = 2Z_0$, and (h) $Z_{L2} = 3Z_0$. $Z_0 = 50\ \Omega$.

D. Case 2 (WPT to Two Devices)

Fig. 7 shows the power transfer efficiency according to the normalized load impedance of Rx coil #1, Z_{L1}/Z_0, for case 2. Fig. 7(a)–(d) represents when the load impedance of Rx coil #2, $Z_{L2} = 0.48Z_0$, Z_0, $2Z_0$, and $3Z_0$, where $Z_0 = 50\ \Omega$. The calculated optimum capacitance values when $Z_{L1} = Z_{L2} = Z_0$ for each IMN are shown in the figure. Measured total power transfer efficiency values η are in good agreement with the calculated results. Since an initial load impedance for matching in each Rx is Z_0, the maximum power transfer efficiency can be obtained at $Z_{L1} = Z_{L2} = Z_0$, as shown in Fig. 7(b) and (f).

With the SP-PS and PS-PS combinations, the power transfer efficiency of Rx coil #1 η_{rx_1} decreases with increasing Z_{L1}, whereas the power transfer efficiency of Rx coil #2 η_{rx_2} increases with increasing Z_{L1}. On the other hand, with the SP-SP and PS-SP combinations, there is little change in η_{rx_1} and η_{rx_2} compared with the SP-PS and PS-PS combinations. This means that stable power transfer efficiency can be achieved with the SP-SP or PS-SP combinations.

From a practical viewpoint, an increase in the load impedance denotes that a Li-Ion battery is almost charged, whereas a decrease in the load impedance represents that a battery is almost discharged. Hence, it should be noted that the use of a PS IMN at Rx is more applicable for a WPT system for charging two devices where more power should be delivered to lower load impedance and lower power is delivered to higher load impedance. In contrast, an SP IMN at Rx sides becomes a good candidate for a WPT system that should be less sensitive to load variation.

SP-SP and PS-SP IMN combinations also have the same power transfer efficiency, whereas SP-PS and PS-PS IMN combinations have the same power transfer efficiency. For this reason, only SP-SP and PS-PS IMN combinations are compared in the next experiment.

E. Case 3 (WPT to Three Devices)

Fig. 8 compares calculated, simulated, and measured power transfer efficiency values with SP-SP and PS-PS IMN combinations based on Z_{L1}/Z_0 for case 3 when $Z_0 = 50\ \Omega$. In this case, cross couplings between the Rx coils, in particular between Rx coils #2 and #3, exist since the Rx coils are placed close to each other, as shown in Fig. 5(c). Simulation results considering cross coupling by the ADS simulation are compared with the measured results. In the simulation, calculated cross-coupling mutual inductances are used as follows: $M_{12} = -36$ nH, $M_{23} = -75$ nH, and $M_{13} = -14$ nH.

In case 3, several scenarios exist depending on load impedance. In this paper, two scenarios of $Z_{L2} = 0.48Z_0$ and $Z_{L3} = 3Z_0$ and $Z_{L2} = 3Z_0$ and $Z_{L3} = 0.48Z_0$ are employed. Load impedances $0.48Z_0$ and $3Z_0$ are regarded as one of the worst cases in wireless charging. The calculated optimum capacitance values when $Z_{L1} = Z_{L2} = Z_{L3} = Z_0$ are also shown in the figure.

In Fig. 8(a) and (b), the calculated power transfer efficiency of Rx coil #1 is the highest followed by that of Rx coil #3 and Rx coil #2; the efficiency changes little, irrespective of variations of Z_{L1}. However, in Fig. 8(b), measured efficiency

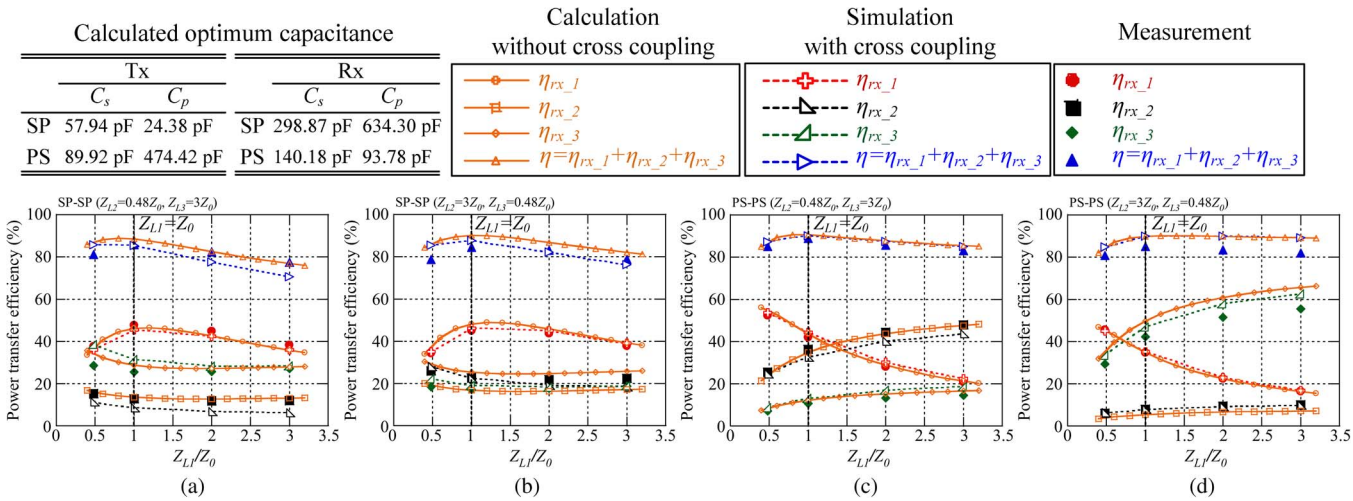

Fig. 8. Comparison of calculated, simulated, and measured power transfer efficiency values, according to the variation of normalized load impedance Z_{L1}/Z_0. (a) With SP-SP IMN combination where $Z_{L2} = 0.48Z_0$ and $Z_{L3} = 3Z_0$, (b) SP-SP IMN combination where $Z_{L2} = 3Z_0$ and $Z_{L3} = 0.48Z_0$, (c) PS-PS combination where $Z_{L2} = 0.48Z_0$ and $Z_{L3} = 3Z_0$, and (d) PS-PS combination where $Z_{L2} = 3Z_0$ and $Z_{L3} = 0.48Z_0$. $Z_0 = 50\ \Omega$.

of Rx coil #2 η_{rx_2} is slightly higher than that of Rx coil #3 η_{rx_3}. This is because cross coupling affects power transfer efficiency values [6], [7]. The simulated results, considering cross-coupling effects, are more consistent with the measured results than with the calculated results, with no consideration of the cross coupling. Nevertheless, the calculated results are mostly in agreement with the measured results.

The PS-PS IMN combination has significantly different characteristics compared with the SP-SP IMN combination. In Fig. 8(c) and (d), η_{rx_1} decreases with increasing Z_{L1}, which is similar to the results using a PS IMN at Rx sides in case 2, whereas η_{rx_2} and η_{rx_3} increase. In Fig. 8(d), Rx coil #2 with $0.48Z_0$ has higher power transfer efficiency than Rx coil #3, although $M_3 > M_2$. An Rx coil with the highest load impedance of $3Z_0$ has the lowest power transfer efficiency in Fig. 8(c) and (d). It should be pointed out that more power to a device with lower load impedance in a WPT system using a PS-PS IMN combination can be transferred regardless of the number of devices. In addition, a WPT system using the PS-PS IMN combination is slightly affected by cross coupling compared with that using an SP-SP IMN combination.

Fig. 9 shows calculated, simulated, and measured power transfer efficiency values when $Z_{L1} = Z_{L2} = Z_{L3} = Z_0$ for case 3. To verify the measurement of S-parameters using a VNA, output power is measured using a spectrum analyzer (HP 8563E) after feeding 23 dBm of power using a function generator (Agilent 33521A). From top to bottom in the figure, each patterned bar denotes η_{rx_1}, η_{rx_2}, and η_{rx_3}. As shown in the figure, the measured results using the VNA are consistent with the calculated results and the measured results using the spectrum analyzer.

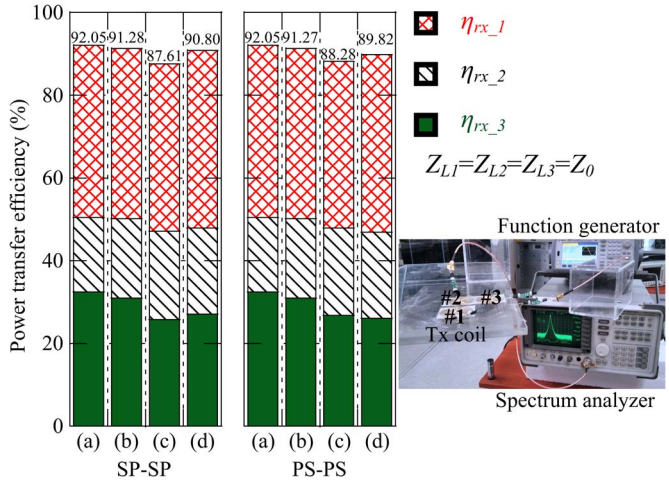

Fig. 9. Comparison of power transfer efficiency values when $Z_{L1} = Z_{L2} = Z_{L3} = Z_0 = 50\ \Omega$ for case 3. (a) Calculation, (b) simulation with cross coupling, (c) measurement using a VNA, and (d) measurement using the function generator and spectrum analyzer.

IV. Conclusion

Power transfer behaviors of WPT systems using capacitive IMNs of SP and PS combinations are reported for charging multiple devices simultaneously using one Tx coil. To design the systems, the optimum capacitance values have been presented for SP-SP, SP-PS, PS-SP, and PS-PS IMN combinations. The theoretical results are well verified with measurement using a VNA, as well as a power source and a spectrum analyzer.

It is shown that, in a WPT system using SP and PS IMNs, WPT behavior according to load variation changes based on the IMN at an Rx. For example, for a WPT system using the PS IMN at an Rx, input power is divided into each device automatically depending on the load impedance of each device. That is, the device of a lower load impedance receives more power. On the other hand, the power transfer efficiency of each device in a WPT system using the SP IMN at the Rx is less sensitive according to load variation where the efficiency is mainly related to mutual inductance between the Tx and Rx coils. Furthermore, using a PS IMN at an Rx is more effective than an SP IMN for reducing the influence of the cross coupling between neighboring Rx coils. It is also pointed out that, since a WPT system for charging multiple devices simultaneously has different characteristics according to the combination of SP and

PS IMNs, as shown in this paper, SP or PS IMNs should be properly adopted depending on the applications.

REFERENCES

[1] A. Kurs *et al.*, "Wireless power transfer via strongly coupled magnetic resonances," *Science*, vol. 317, no. 5834, pp. 83–86, Jul. 2007.

[2] A. P. Sample, D. T. Meyer, and J. R. Smith, "Analysis, experimental results, range adaptation of magnetically coupled resonators for wireless power transfer," *IEEE Trans. Ind. Electron.*, vol. 58, no. 2, pp. 544–554, Feb. 2011.

[3] M. P. Kazmierkowski and A. J. Moradewicz, "Unplugged but connected: Review of contactless energy transfer systems," *IEEE Ind. Electron. Mag.*, vol. 6, no. 4, pp. 47–55, Dec. 2012.

[4] X. Liu and S. Y. R. Hui, "Optimal design of a hybrid winding structure for planar contactless battery charging platform," *IEEE Trans. Power Electron.*, vol. 23, no. 1, pp. 455–463, Jan. 2008.

[5] D. Kurschner, C. Rathge, and U. Jumar, "Design methodology for high efficient inductive power transfer systems with high coil positioning flexibility," *IEEE Trans. Ind. Electron.*, vol. 60, no. 1, pp. 372–381, Jan. 2013.

[6] D. Ahn and S. Hong, "Effect of coupling between multiple transmitters or multiple receivers on wireless power transfer," *IEEE Trans. Ind. Electron.*, vol. 60, no. 7, pp. 2602–2613, Jul. 2013.

[7] K. K. Ean, B. T. Chuan, T. Imura, and Y. Hori, "Impedance matching and power division algorithm considering cross coupling for wireless power transfer via magnetic resonance," in *Proc. IEEE INTELEC*, 2012, pp. 1–5.

[8] C.-S. Wang, O. H. Stielau, and G. A. Covic, "Design considerations for a contactless electric vehicle battery charger," *IEEE Trans. Ind. Electron.*, vol. 52, no. 5, pp. 1308–1314, Oct. 2005.

[9] G. A. Covic, "Inductive power transfer," *Proc. IEEE*, vol. 101, no. 6, pp. 1276–1289, Jun. 2013.

[10] S. Hasanzadeh, S. Vaez-Zadeh, and A. H. Isfahani, "Optimization of a contactless power transfer system for electric vehicles," *IEEE Trans. Veh. Technol.*, vol. 61, no. 8, pp. 3566–3573, Oct. 2012.

[11] T. C. Beh, M. Kato, T. Imura, S. Oh, and Y. Hori, "Automated impedance matching system for robust wireless power transfer via magnetic resonance coupling," *IEEE Trans. Ind. Electron.*, vol. 60, no. 9, pp. 3689–3698, Sep. 2013.

[12] A. P. Sample, B. H. Waters, S. T. Wisdom, and J. R. Smith, "Enabling seamless wireless power delivery in dynamic environments," *Proc. IEEE*, vol. 101, no. 6, pp. 1343–1358, Apr. 2013.

[13] S. G. Lee, H. Hoang, Y. H. Choi, and F. Bien, "Efficiency improvement for magnetic resonance based wireless power transfer with axial-misalignment," *Electron. Lett.*, vol. 48, no. 6, pp. 339–340, Mar. 2012.

[14] K. A. Grajski, R. Tseng, and C. Wheatly, "Loosely-coupled wireless power transfer: Physics, circuits, standards," in *Proc. IEEE MTT-S Int. IMWS-IWPT*, 2012, pp. 9–14.

[15] Wireless Power Consortium Standards, System description wireless power transfer, volume I: Low power part 1: Interface definition version 1.0.2, Apr. 2011.

[16] J. Lee, Y.-S. Lim, W.-J. Yang, and S.-O. Lim, "Wireless power transfer system adaptive to change in coil separation," *IEEE Trans. Antennas Propag.*, vol. 62, no. 2, pp. 889–897, Feb. 2014.

[17] L. Chen, S. Liu, Y. C. Zhou, and T. J. Cui, "An optimizable circuit structure for high-efficiency wireless power transfer," *IEEE Trans. Ind. Electron.*, vol. 60, no. 1, pp. 339–349, Jul. 2013.

[18] W.-S. Lee, H. L. Lee, K.-S. Oh, and J.-W. Yu, "Switchable distance-based impedance matching networks for a tunable HF system," *Prog. Electromagn. Res.*, vol. 128, pp. 19–34, May 2012.

[19] Y. Lim, H. Tang, S. Lim, and J. Park, "An adaptive impedance matching network based on a novel capacitor-matrix for wireless power transfer," *IEEE Trans. Power Electron.*, vol. 29, no. 8, pp. 4403–4413, Aug. 2014.

[20] A. Kurs, R. Moffatt, and M. Soljačić, "Simultaneous mid-range power transfer to multiple devices," *Appl. Phys. Lett.*, vol. 96, no. 4, 2010.

[21] J. Park and S. Nam, "Analysis of wireless power transfer characteristics for multiple receivers by time sharing technique," *J. Korean Inst. Electromagn. Eng. Sci.*, vol. 11, no. 3, pp. 183–185, Sep. 2011.

[22] B. L. Cannon, J. F. Hoburg, D. D. Stancil, and S. C. Goldstein, "Magnetic resonant coupling as a potential means for wireless power transfer to multiple small receivers," *IEEE Trans. Power Electron.*, vol. 24, no. 7, pp. 1819–1825, Jul. 2009.

[23] J. Kim, H.-C. Son, D.-H. Kim, K.-H. Kim, and Y.-J. Park, "Analysis of wireless energy transfer to multiple devices using CMT," in *Proc. APMC*, 2010, pp. 2149–2152.

[24] J. Kim, H.-C. Son, D.-H. Kim, and Y.-J. Park, "Impedance matching considering cross coupling for wireless power transfer to multiple receivers," in *Proc. IEEE WPT*, 2013, pp. 226–229.

[25] M. Chen and G. A. Rincon-Mora, "Accurate, compact, power-efficient Li-Ion battery charger circuit," *IEEE Trans. Circuits Syst. II, Exp. Briefs*, vol. 53, no. 11, pp. 1180–1184, Nov. 2006.

[26] C.-J. Chen and T.-H. Chu, "Virtual auxiliary termination for multiport scattering matrix measurement using two-port network analyzer," *IEEE Trans. Microw. Theory Tech.*, vol. 55, no. 8, pp. 1801–1810, Aug. 2007.

Jinwook Kim (S'11–M'14) received the B.S. degree in electronic engineering from Ajou University, Suwon, Korea, in 2009 and the Ph.D. degree in power electrical equipment information and communications engineering from the University of Science and Technology, Ansan, Korea, in 2014.

Since September 2014, he has been with the Korea Electrotechnology Research Institute, Ansan, as a Postdoctoral Researcher. His research interests include electromagnetic theory and wireless power transfer.

Dr. Kim was a recipient of the Best Paper Award at the IEEE Microwave Theory and Techniques Society International Microwave Symposium Series-Innovative Wireless Power Transmission in 2011.

Do-Hyeon Kim (S'13) received the B.S. degree in electronic engineering from Yonsei University, Seoul, Korea, in 2009. He is currently working toward the M.S. and Ph.D. degrees in power electrical information and communications engineering at the University of Science and Technology, Ansan, Korea.

He is also with the Korea Electrotechnology Research Institute, Ansan. His research interests include microwave and millimeter-wave antennas and wireless power transfer.

Young-Jin Park (M'03) received the B.S. degree from Chung-Ang University, Seoul, Korea, in 1997, the M.S. degree in electrical engineering from the Korea Advanced Institute of Science and Technology, Daejeon, Korea, in 1999, and the Dr.-Ing. (Ph.D.) degree in electrical engineering and information technology from the University of Karlsruhe (currently Karlsruhe Institute of Technology), Karlsruhe, Germany, in 2002.

From March 2002 to October 2002, he was a Research Associate with the Institut für Hochfrequenztechnik und Elektronik (IHE). In November 2002, he joined the Korea Electrotechnology Research Institute, Ansan, Korea, where he is currently a Principal Researcher. Since March 2005, he has also been an Adjunct Professor with the University of Science and Technology, Ansan. His research interests include high-resolution impulse radio-based ultrawideband (UWB) sensors (UWB real-time location systems, ground-penetrating radar, and time-domain reflectometry), wireless power transfer based on magnetic resonance and microwaves, and millimeter-wave antennas and propagation for automotive radar.